STAR Note 263

Studies of Several Wire and Pad Configurations for the STAR TPC.

W. Betts (Univ. of Texas at Austin), W. Gong (Max Planck Institute, Munich), E. Hjort (Purdue) and H. Wieman (LBNL)

Introduction

The final state of a heavy-ion collision at RHIC can have several thousand particles emitted. To track charged particles in such a high-multiplicity event, a large-volume Time Projection Chamber (TPC) is to be used in the STAR experiment.[1] The STAR TPC has a cylindrical geometry with one central membrane cathode and two-end-caps. The central cathode and inner and outer field cages provide the drift E-field. The end-caps contain thin-gap, multiwire proportional chambers (MWPCs) with a pad plane readout surface on the outermost cathode surface. For each segment of an ionized track, the primary signal electrons are multiplied by avalanches near the anode wires, and image charges are induced on the array of small pads near the anode wires. The amplitudes of these signals are digitized as a function of time. Measurement of the drift time allows determination of the z-coordinate (perpendicular to the MWPC and parallel to the RHIC beam), while the pads provide the (x, y) coordinates (perpendicular to the beam). This three-dimensional tracking capability of a TPC allows determination of individual momenta of charged particles by tracking them through a solenoidal magnetic field and identifying them with multiple energy-loss (dE/dx) measurements.

Design of the end-cap TPC is critical to achieve the optimum performance for STAR with respect to spatial resolution, operational stability and dynamical range. We have undertaken a series of investigations, including both measurements and calculations, to study issues such as gas-gain characteristics, pad-response functions, pad signal amplitude, shaping-time effects, wire displacement, signal timing and electrical stability. For the purposes of these tests, several small multiwire proportional chambers with cathode (pad) readouts have been built. The primary differences between chambers are in the wire geometries, such as varying wire heights and the presence of field wires interspersed among the anode wires. Additionally, tests have been performed on larger chambers that more accurately represent the STAR configuration for some purposes. These systematic studies have helped us finalize the design of the STAR TPC MWPCs and pad plane layouts.

TPC Sector Design

Each TPC end-cap is divided into 12 identical super-sectors. Each super-sector consists of an outer sector and an inner sector. Figure 1 shows the final design of the pad plane in one super-sector. It shows the actual distribution of pads and geometrical dimensions. The outer sector has 3940 rectangular pads of 6.2mm by 19.5mm in size which are arranged in 32 rows. The inner sector has 1750 rectangular pads of 2.85mm by 11.5mm arranged in 13 rows.

There are three wire planes positioned above the pad plane, with every wire stretched under proper tension, sufficient to insure that they will not deflect from their nominal positions oriented parallel to the pad rows. In the inner (outer, respectively) sector, the anode wire plane consists of 20μm diameter gold-plated tungsten wires with a 4mm pitch located 2mm (4mm) above the pad plane. The smaller wire spacing and pad size of the inner sectors provides better spatial resolution necessary for tracking resolution near the center of the detector where track density is highest. The ground wire plane consists of 75μm diameter beryllium-plated copper wires with 1mm pitch, located 4mm (8mm) above the pad plane. Finally, the gating-grid wire plane consists of 75μm diameter beryllium-plated copper wires with 1mm pitch, 14mm (18mm) above the pad plane. The gating-grid plays no direct role in the signal generation or tracking and should not affect the TPC performance. As its name implies, it acts as a gate. When it is uniformly biased, it is open and the TPC will receive drifting electrons. To close the gate, alternating wires of the gating grid will be brought to different potentials, such that drifting electrons will terminate on the gating grid rather than reaching the avalanche region near the anode. It is worth pointing out now that we have decided not to use

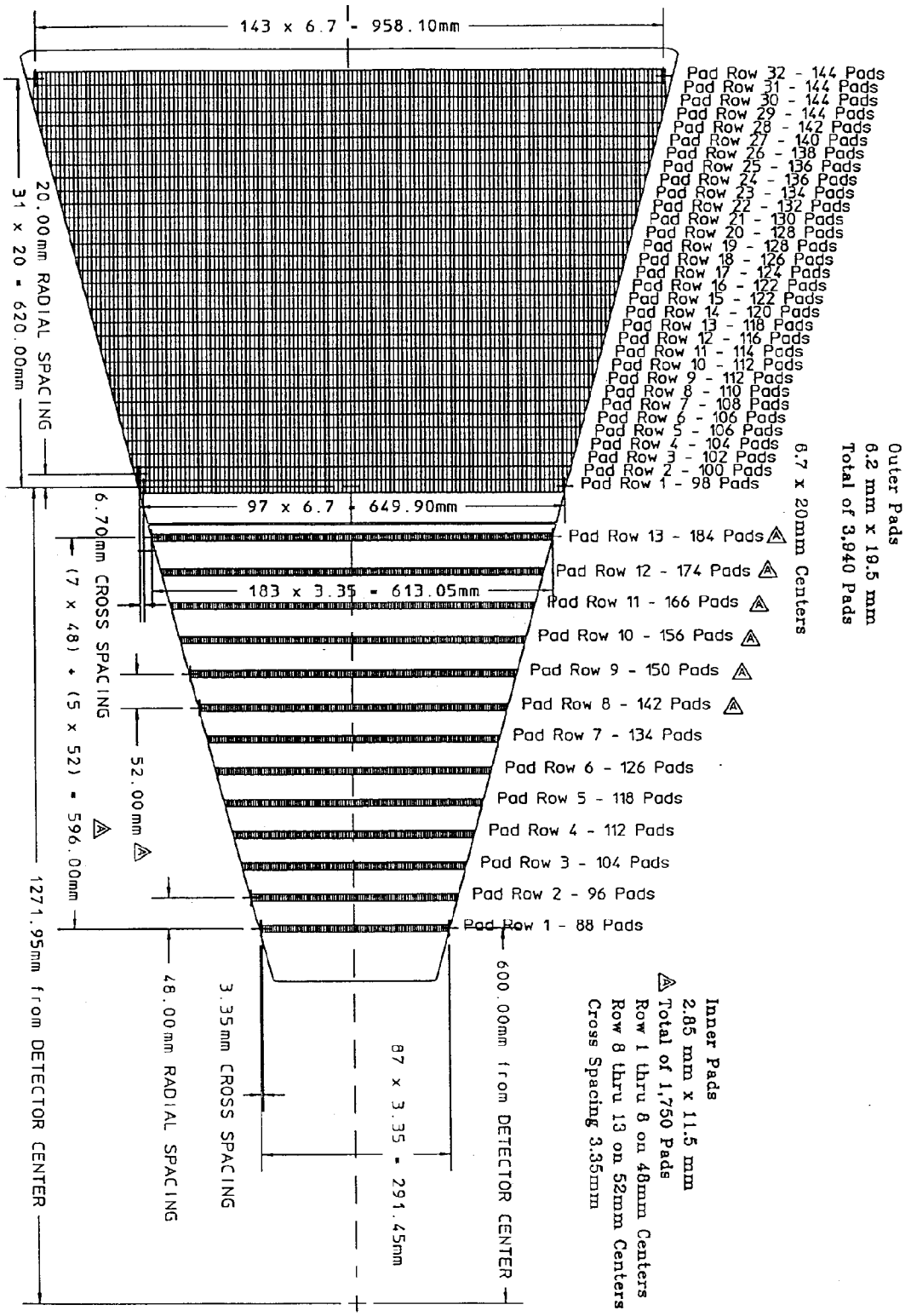

Figure 1. Padplane layout for one super-sector.

field wires (grounded wires between the anode wires) in the STAR TPC for simplicity's sake; some further justification for that decision will be included later in this paper. We have seen that performance of the TPC is not compromised by this decision to any appreciable extent within our operating regime and may, in fact, be slightly enhanced.

Small Test Chamber Construction

Building one of the small chambers began with creating the pad plane cathode surface. The pad planes were made with copper-plated nema-G10 using standard PC board techniques. Of the six chambers built, five have pad layouts identical to the specifications for the STAR TPC inner sectors. (As shown in figures 1 and 2.) Each inner sector pad is 2.85 mm wide by 11.5 mm long, with a 0.5 mm gap between adjacent pads. In these small chambers there are two rows of eighteen pads. The rest of the pad plane surface is copper-plated and is grounded in the final set-up. The pad plane PC board includes plated vias and traces from each pad to the backside where a surface mounted connector allows readouts from each pad individually. The sixth chamber is a small replica of the STAR TPC outer sectors with three rows, with nine pads each, each pad being 6.2 mm wide by 19.5 mm long separated from its neighbors by 0.5mm.

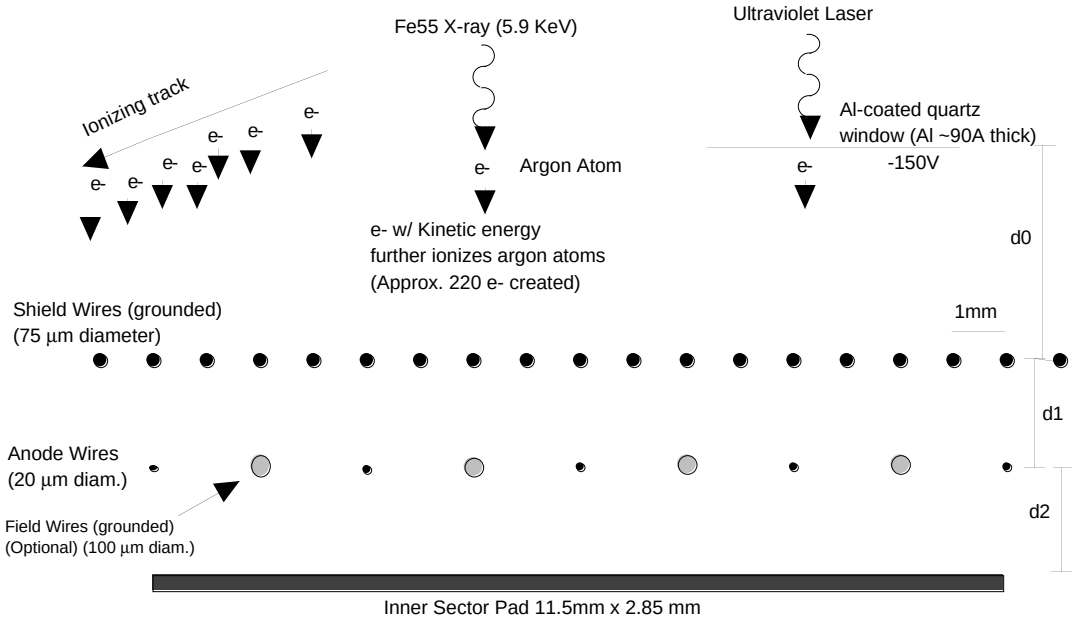

Figure 2. The chamber layout as seen looking parallel to the wires including the optional field wires (lightly shaded). Also shown are the various methods used to generate signals.

Once the pad planes were completed, the wires were put on. The first plane of wires is the anode plane, as described above. (See figure 2.) Frames of wires with 4mm spacing were taken from the STAR project's wire-winding machine, which insures proper spacing and tension. The height of the anode wires above the pad plane is one of the important variables that differentiate these chambers. Of the pad planes with inner sector pads, one was built with 1.5mm between the pad plane and anode wires (d2 in figure 2), three with 2mm (each one unique in ways to be described below) and one with 4 mm spacing. The chamber with outer sector pads has 4mm spacing (d1 and d2) to match the STAR TPC outer sector design. Small blocks of nema-

G10, slightly shorter than the desired wire heights, were epoxied to the pad plane. Precision-ground glass rods were made of the desired diameters to set the wire heights. These glass rods were placed outside the nema-G10 supports and then the frames with wires were lowered onto the glass rods until the wires rested on them. The wires were lined up so that an anode wire would be directly over the center of each pad. With the wires supported slightly above the nema by the glass rods, epoxy was poured over the wires onto the nema and encapsulated each wire. On one of the nema supports, a narrow piece of copper (conductive) tape was laid under the wires. Each anode wire was soldered to this tape and a cable was attached which is later hooked up to the anode high voltage power supply and to readout-electronics to see the signals on the anodes (all ganged together through the copper tape). The wires were then cut from the frame and the ends snipped off. To alleviate the danger of discharge from these exposed ends, they were epoxied over as well as the copper tape and solder joints. With the anode wires firmly held in place by the epoxy, the glass rods were removed. Of the three chambers with 2mm pad-anode spacing, one has additional field wires in between the anode wires as shown in figure 2. These field wires are grounded and they have a diameter of 100μm.

The second plane of wires (called shield wires) is grounded and was put on in a way very similar to the procedures used for the anode wires. These wires have a pitch of 1mm. The usual arrangement in this type of detector is for the distance from the shield wires to the anode wires to be the same as the distance between the anode wires and the pad plane (that is, having a symmetry of the cathode surfaces about the anode wires). Five of our chambers have such an arrangement, but the third chamber with 2mm pad-anode spacing was excepted. It has a 3mm gap from the anode wires to the shield wires. Most of the above work was done in a clean room. Once completed, each unit was showered in a high-pressure spray of warm water and detergent, rinsed with tap water and finally rinsed with de-ionized water. They were then placed in an oven for 2-3 hours at 150° F to dry.

To summarize, and to introduce some shorthand, we have made six chambers, to be denoted as 1.5-1.5, 2-2, 2-2fw, 2-3, 4-4 and 4-4o. These indicate the pad-anode distance and the anode-shield distance as d2-d1, as well as indicating different configurations with identical wire spacings. The 2-2fw is the chamber with field wires and 4-4o is the chamber with the STAR TPC outer sector design. Further on, additional geometries will be mentioned with the same sort of shorthand notation. These small chambers do not include a gating-grid layer, because it is expected that it would have no appreciable effect on the performance characteristics that we are studying.

Small Chamber Measurement Set-up

Many of the measurements on the small chambers are similar to, or follow from, those done by H. Huang, *et al*[2]. All measurements were done with P10 gas (90% Argon, 10% Methane). This is a common gas for these types of chambers and is one of the gases intended for use in STAR. These small chambers are housed in aluminum boxes that can be sealed effectively with tape. To maintain a good gas quality, a small, constant flow of P10 was used. The exhaust gas was monitored and always showed below 50ppm H_2O during measurements. For tests in which precise gas gain was an important factor, less than 30ppm was considered sufficient. With a permanent epoxy seal, it was possible to get below 10ppm with a relatively low flow rate. It is assumed that the pressure was slightly higher than atmospheric pressure and that the temperature was equal to the room temperature. Temperature and pressure variations do affect gas gain.[3] We did not monitor these explicitly, but we are able to estimate their effect based on typical lab environment changes and the effect is very small.

In the small chambers, signals on the anode wires can be read-out with the circuit and electronics shown in figure 3, which also allow the input of high voltage to the anodes and

provide some protection against discharge. Note that all the anode wires are connected together, unlike the STAR TPC, in which individual wires can be read out. However, the anode wires in the STAR TPC will not be used for particle tracking because of the high multiplicity of STAR events and the wire lengths, but they are still useful as a measure of the total energy loss rate of charged particles and may be useful in the triggering scheme. Individual anode signals are also used for verifying the performance of STAR sectors when they are built. In all measurements, the shield wires and unused pads are directly grounded to avoid charge build-up that would affect the field. Positive voltage is supplied to the anode wires, and the current drawn may be monitored.

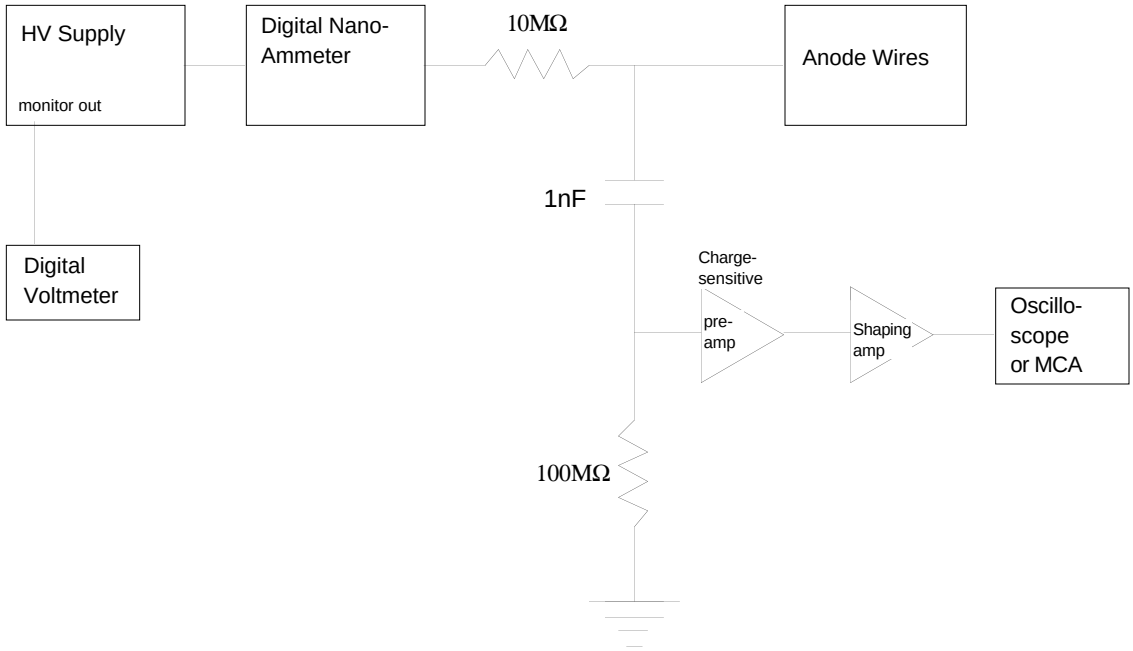

Figure 3. Anode voltage supply and anode signal readout set-up.

We have three different methods of inducing signals, all based on some form of ionizing radiation, illustrated in a simplified way in figure 2. The leftmost one is the actual type of signal generation during STAR's data collection. Charged particles traversing the drift gas region may leave behind a track of electrons. The drift field created by the field cage and central membrane will drift these electrons toward the sectors on the end-caps where data collection occurs. To measure gas gain and the effect of changes in read-out electronics, we typically used an Fe-55 x-ray source. These soft x-rays have an energy of 5.9keV and they typically liberate one electron with kinetic energy from an Argon atom. This low energy β-ray then produces approximately 225 electrons through further ionization in the P10. The third method of signal creation uses a 337nm nitrogen laser focused on a thin aluminum-coated (~90Angstroms) window. The window is approximately 1cm from the ground plane and has a bias of -150V to push the liberated electrons toward the wire planes. The use of the laser allows a very small signal source size and precise positioning used for measurements of pad response functions and pad-anode coupling. More detail will be given below in the sections describing the individual measurements.

Gas Gain and Field Strength

The first measurements done were to determine the gain as a function of the anode voltage. The relationship between gain and voltage depends on the geometry used, so each of our chambers is measured separately. We first calibrate the readout electronics by injecting a known amount of charge at the preamplifier input through a precision capacitor. With this calibration, we are able to determine the number of electrons arriving at the anode wire after an avalanche. As mentioned earlier, we also know that an Fe-55 x-ray will produce approximately 225 electrons before the avalanche. The gas gain is then the number of avalanche electrons divided by 225. An Fe-55 source emitting 5.9keV x-rays is placed over the chamber. Putting the amplified signals from the anode wires into an MCA produces the spectrum shown in figure 4. It shows the primary peak, as well as the escape peak characteristic of argon gas (in which only about 110 electrons reach the avalanche region). The energy resolution indicated by this spectrum is about 24% FWHM. This is typical of all of our chambers.

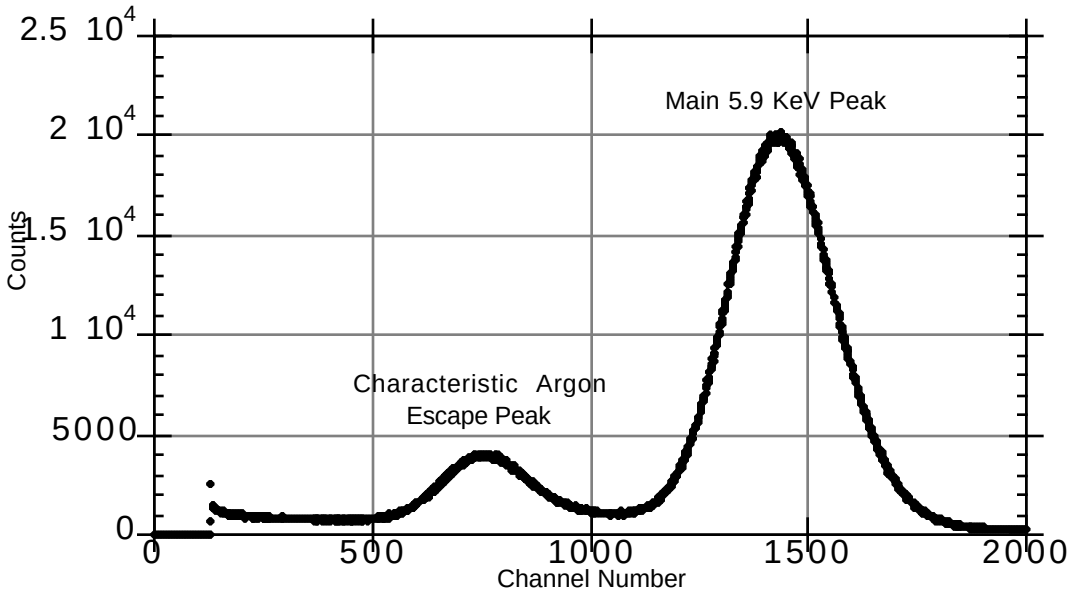

Figure 4. Typical Fe-55 spectrum in P10 gas from one of the chambers. There is noise discrimination below channel 150.

By determining the position of the main peak, we may determine the gas gain through our calibration. Varying the anode voltage and repeating the measurement provides the data shown in figure 5. An exponential curve of the form

$$G = e^{b\cdot(V-V_0)} \qquad (1)$$

is fit to the data for our small chambers. The parameters b and V_0 of the curve fits for each chamber are included in Table 1 at the end of this paper. Additionally in figure 5, we have included some similar measurements performed on the EOS prototype. However, figure 5 does not have the actual gas gain, because we used a short peaking time (200ns) for our shaping electronics to more closely duplicate STAR's front-end electronics (with a peaking time of

approximately 125ns) and were effectively ignoring some of the signal on the anode wires. Increasing the shaping time to several microseconds and measuring the gain showed that our gain measurements are about 25-30% below the actual gas gain. So figure 5 shows the effective gain with the 200ns rise time. STAR's front-end electronics pre-amp shaper chip has a 125ns rise time. From our measurements, we have visually extrapolated down to this time as shown in figure 6.

From figure 5, we see that the gas gain becomes higher at a given voltage as the anode to cathode distance decreases. This is as one would expect because the electric field near the wires varies inversely with the anode-cathode spacing. Furthermore, the presence of field wires increases the gain, again as a result of an increased field at the anode wires. With these systematic measurements of the gain, we are interested in finding an expression with which we can obtain the gain for a given field strength at the wire surface. We have used GARFIELD[4] to calculate the field strengths at the surfaces of the anode wires at two different voltages for each chamber. The field strengths are then correlated with the measured gains as shown in figure 7. This data was well fit by the equation

$$G = G_0 e^{(c \cdot E_g)} = e^{(c \cdot (E_g - E_{g0}))} \qquad (2)$$

with c = 0.0757 cm/kV and G_0= 0.000844 or E_{g0}= 93.5 kV/cm. With these parameters, it should be possible to approximately calculate the gas gain for any MWPC with any wire geometry in P10 gas just from calculating the field at the surface of the anode wires.

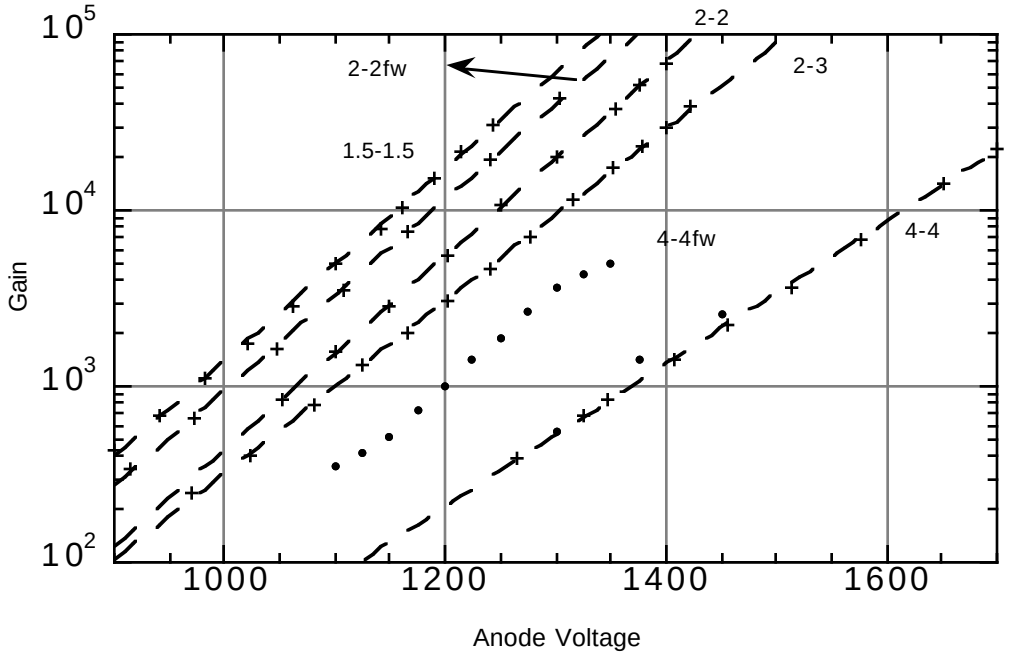

Figure 5. Gain curves for the various chambers, showing data points (crosses) and exponential curve fits. Also included are data (unfitted dots) from the EOS TPC prototype.

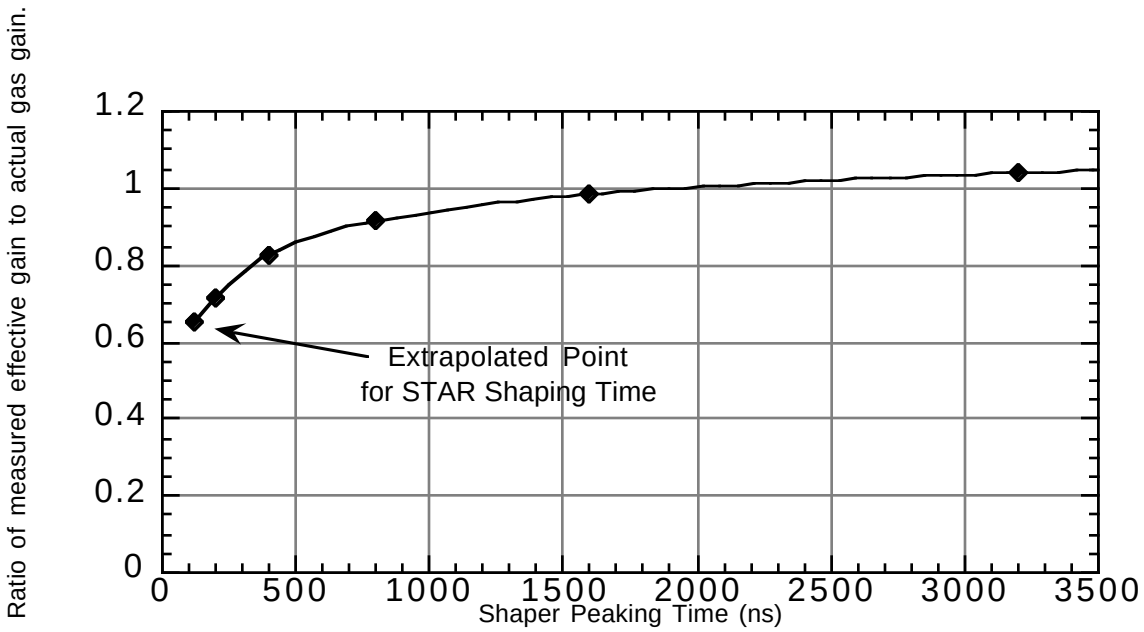

Figure 6. The effect of electronics peaking time on measured signal amplitude. The far left point is an extrapolated estimate of STAR's effective gain based on the 125ns peaking time of the front-end electronics.

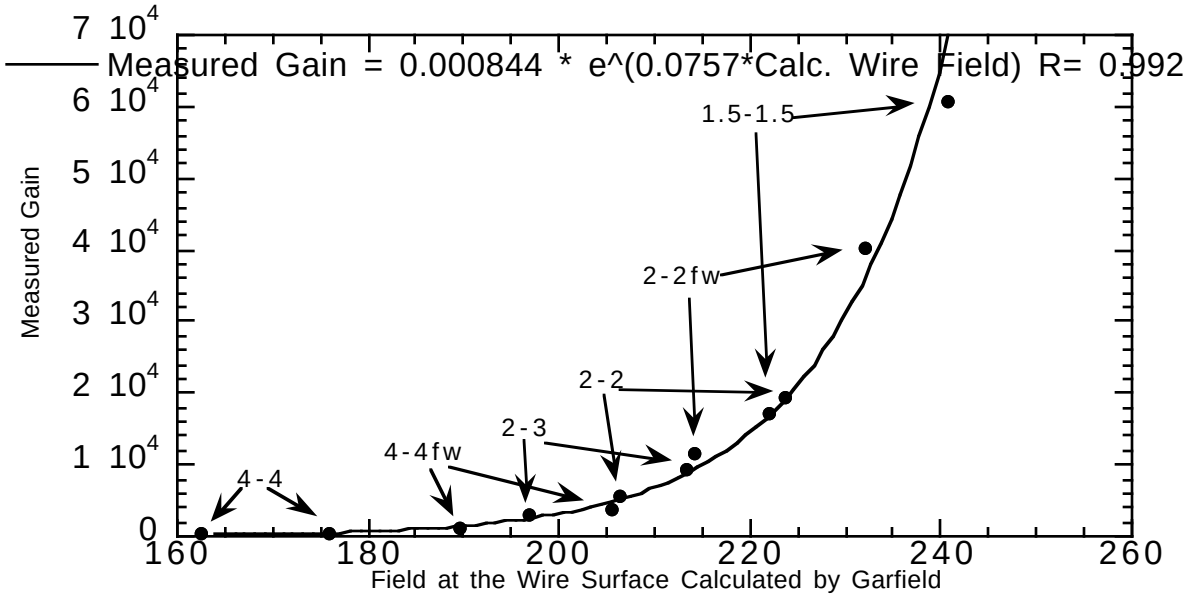

Figure 7. The different wire spacings were input into Garfield at two different voltages and compared to the measured gains at the same voltages. The curve is a best-fit exponential.

Pad Response Function

The two primary measurements from the TPC are dE/dx and particle tracking. The gain stability and energy resolution affect the first. Position resolution for particle tracking is affected by such things as electron cloud diffusion in the drift region and the distribution of induced charge on the pad plane. Electron diffusion has been measured extensively (see for instance Alber, et. al.[5]) For determining the charge distribution on the pad plane, we have made several measurements and calculations. The pad response function (PRF) relates the signal induced on a pad to the position of a track parallel to the length of a pad. (Tracks with some angle to the pad length can be handled also.) The width of the PRF is a key measure of the position resolution of a TPC. The case with symmetric cathode spacing about the anodes without field wires is worked out by Blum and Rolandi[6] using the method of images. They determine the induced charge density on an infinite plane (the pad plane) as if both cathode surfaces are infinite planes (although our top plane is a wire plane, this should introduce only a small error.) They express the PRF as the integral of the total induced charge density $\sigma(x)$

$$P_0(x) = \int_{x-W/2}^{x+W/2} \sigma(x')dx' \qquad (3)$$

where $\sigma(x)$ is given by

$$\sigma(x) = -\frac{\lambda}{\pi}\sum_{k=0}^{\infty}(-1)^k \frac{(2k+1)D/2}{x^2 + (2k+1)^2 D^2/4}$$

$$= -\frac{\lambda}{2D}\frac{1}{\cosh(\pi x/D)} \qquad (4)$$

Here λ is the linear charge density of the track, D is the distance between the cathode surfaces (with the assumption that the anodes are exactly in the middle), W is the pad width and x is the distance from the center of a pad to a track projected downward onto the pad plane. This method can be generalized to unsymmetric geometries (still without field wires), though a closed form is not obvious:

$$P_{us}(x) = -\left(\frac{\lambda}{\pi}\right)\int_{x-W/2}^{x+W/2}\left(\sum_{k=0}^{\infty}(-1)^k \frac{\left(2\cdot\left[\frac{k+1}{2}\right] + (-1)^k \cdot c\right)\cdot D}{x'^2 + \left(2\cdot\left[\frac{k+1}{2}\right] + (-1)^k \cdot c\right)^2 \cdot D^2}\right)dx' \qquad (5)$$

in which [y] is the greatest integer function of y and the height of the anode wires above the padplane is given by cD (in the symmetric case, c = 0.5 in which case the summation term simplifies to that given in Eq. 4.) These PRFs can be closely approximated by a Gaussian curve

$$P_0(x) \approx e^{-x^2/2s_0^2} \qquad (6)$$

to which it is relatively easy to fit curves. Using a computer to do the calculations of Eq. 5 (usually out to 1000 terms in the summation), we are able to calculate the expected pad response function and width (as the σ of a Gaussian) for any chamber geometry (without field wires).

In addition to the calculations, we have measured PRFs for all of our chambers using a nitrogen laser on an aluminum coated quartz window as an approximate point source. A fiber-optic cable from the laser was mounted on a precision 3-D translation set-up and brought to focus on the bottom of the window. The laser was scanned across the pad in 0.5mm increments. At each position, the amplitudes of the signals on the anodes and on a pad were measured and the pad to anode signal ratio computed. This is then plotted versus the laser position and the data is fit by a Gaussian. Figure 8 shows a sample of this measurement and curve fit for the 2-2 chamber. The width of the pad response function can be determined from this measured width by subtracting out (in quadrature) the laser spot size width (measured to have an approximate sigma of 0.3 mm) and diffusion width (determined by the drift distance (from 1 cm to 1.5 cm in the small chambers) and the drift field. In addition to the measurement by scanning, we can fix the laser's position over one pad and read out that pad and its neighbors. It does not take a very large signal for three (inner sector) pads to get sufficient signal for measurements, but for five pads, a large signal was required. With so few points, the error upon fitting a Gaussian is larger, but this method was in good agreement with the measurements made while scanning the laser. Table 1 (at the end of this paper) includes the calculated PRF widths and the measured widths for several chambers. Figure 9 shows the computed PRF width (in the symmetric case) as a function of D/2, as well as our measured values. Additionally, we looked for variations in the PRF with different signal sizes and gains. Though not entirely ruled out, the effect appeared to be very small, such that for the range of signals in the STAR TPC, no significant variation is expected.

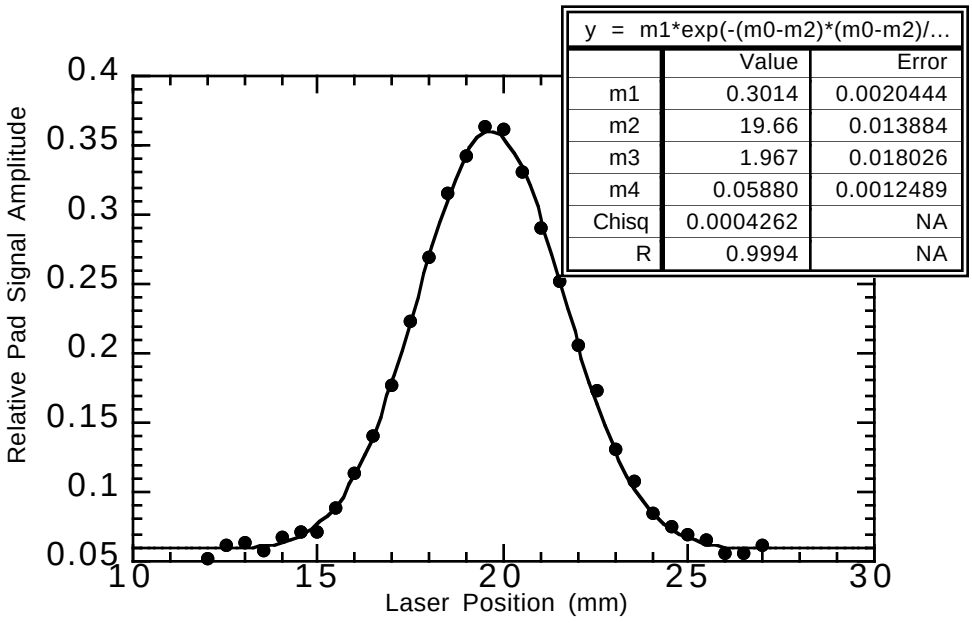

Figure 8. This is a sample of the measurement of the pad response function (PRF) widths. The curve fit is a Gaussian with an offset. m1 is the peak amplitude, m2 is the location of the centroid, m3 is the sigma in mm and m4 is the offset. This particular measurement was done on the 2-2 chamber at a gain of about 1600.

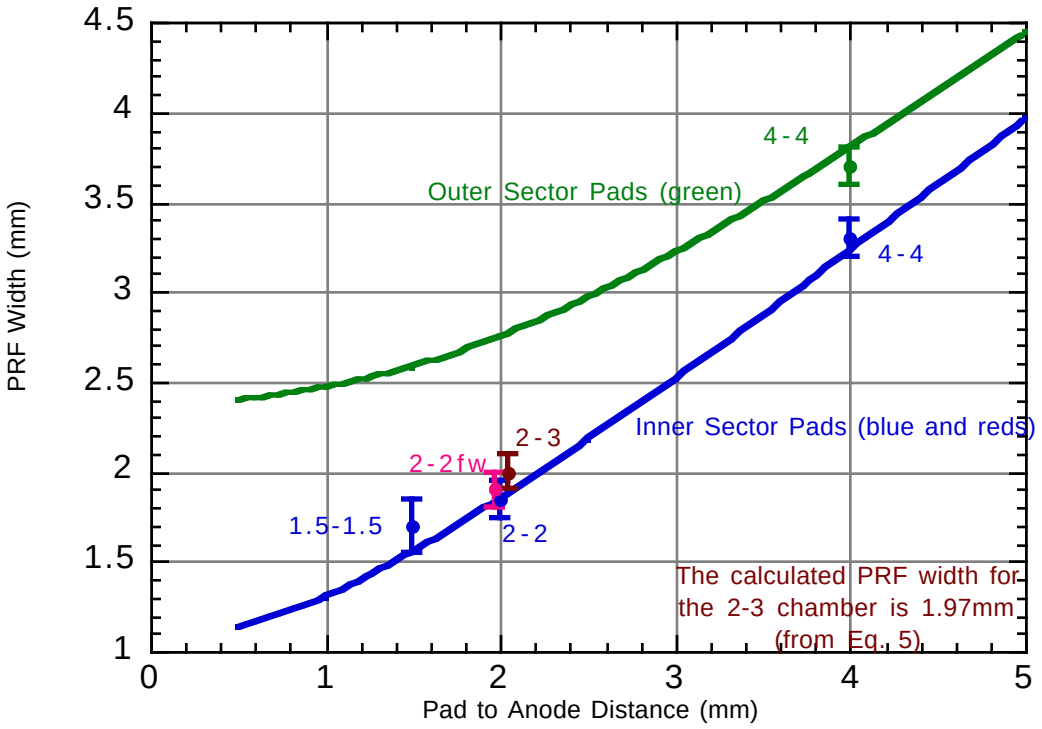

Figure 9. Pad response function widths (sigma of a Gaussian). The solid curves show the calculated values from Eqs. 3. Data points are as measured in small chambers. The 2-2fw and 2-3 data points have been slightly offset left and right for better visual clarity.

Pad Signal Amplitude

In addition to the width of the signals induced on the pad plane, there is the issue of the amplitude. The amplitude determines how many pads will have signals above the threshold of the readout electronics. If the amplitude of the induced signals are small, then some 'hits' will only be seen by two pads and the position determination will suffer as a result. Equation 5 allows an estimate of the induced signal on the pads as a ratio of pad signal to anode signal, assuming the 'hit' is directly over the center of the pad. Though not quite as good an approximation as for the width (for instance, Eq 5 assumes infinitely long pads), it should still be within a few percent of the actual value. Using the nitrogen laser focused directly over a pad, we are able to measure the pad to anode signal ratio for the various chambers by measuring the pad signal and anode signal with the same electronics. The calculated and measured values are given in Table 1. Figure 10 shows our measurements and the calculated pad to anode ratio as a function of pad to anode distance. The larger signal from the chamber without field wires is an important point. It allows a lower operational gain to get the same signal on the pads than using a design with field wires.

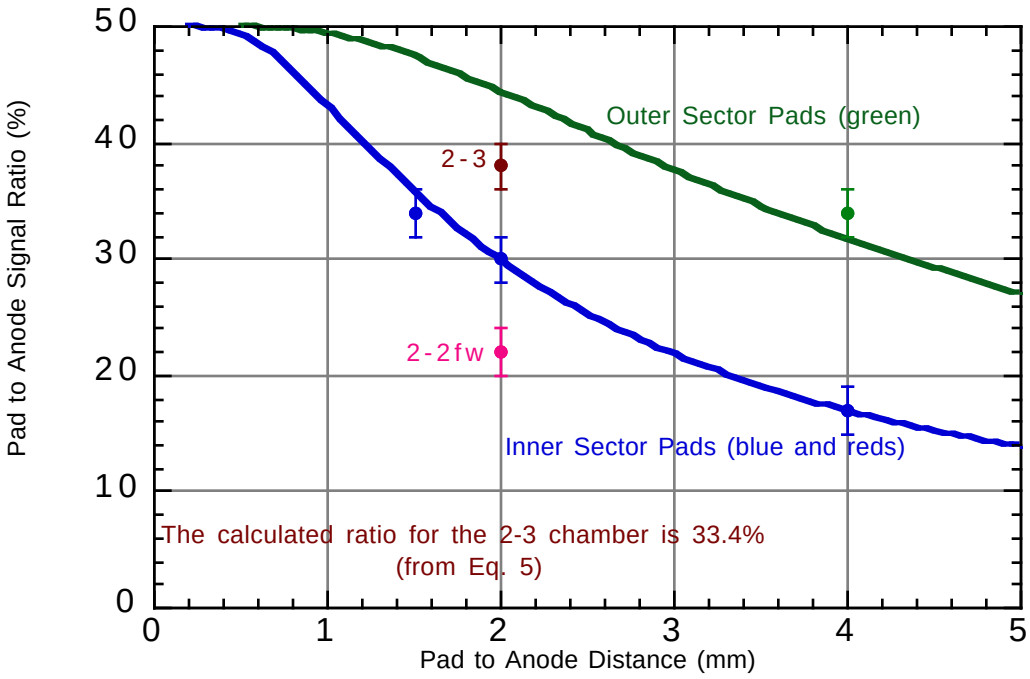

Figure 10. Pad to Anode signal ratios as calculated from Eqs. 3 (curves) and as measured in the small chambers.

Stability

Wire chamber instability usually becomes an issue when one wants to install anodes and cathodes in compact geometries or operate with high gains. We first studied wire instability for the STAR TPC in order to understand the consequence of eliminating field wires.[7] Using the GARFIELD simulation program, we can calculate the wire displacement and gain variation as functions of the anode voltage for various chamber geometries. The magnitudes of wire displacement and gain variation are estimated by considering the equilibrium balance between electrostatic forces and wire tension. A test structure for wire displacement was built to verify our calculations. The agreement between the measurements and calculations has led us to adopt the same method for optimizing the wire spacings for the STAR TPC inner sectors, where a smaller gap between the anode wires and pads is called for. In addition to this mechanical stability, there is also the issue of electrical stability, including such phenomena as sparking, glow discharge, and multiple counting. When encountered, these effects can lead to spurious results and potentially shorten the lifetime of the detector.

Applying voltage bias to the sense wires can displace them from their original (zero bias) positions. Estimating the magnitude of the wire displacement can be done using the method of images. The pad plane was assumed to be a continuous, perfect conductor. For a given voltage on the anodes, we used GARFIELD to calculate the electrostatic charges on the sense and ground wires. We then calculated the electrostatic forces exerted on one anode wire by all other anode wires, sense wires and their images (about the pad plane). Using the tension on the wires, we are able to calculate the displacement.

To verify our calculated displacements, we built a special setup consisting of a metal slab with two wire planes stretched above the metal slab. The sense wire plane has a diameter of 20μm at 4mm pitch and is 2.2mm above the metal slab. The ground plane has 75μm diameter wires at 1mm pitch 4.4mm above the metal slab. (This is almost identical to the STAR TPC outer sector design, with slightly larger spacings.) All of the wires are approximately 1m long. The metal slab and ground wire plane were kept at ground potential while the anode plane was biased. The displacement of an anode wire was then measured using a microscope. Measurements were done at several anode voltages and on twelve anode wires. Figure 11 shows the measured displacement towards the metal slab for one of the central anode wires and the calculated displacements at two tension values, T = 23g and T = 50g. (The wires had a measured tension of 23g, while the STAR requirement calls for 50g.) Furthermore, we compared the wire displacements and wire tensions for all twelve wires at 1600V. This is shown in figure 12. Not surprisingly, there is a clear correlation between wire displacement and wire tension. On the basis of the agreement between our calculations and measurements shown in figure 11, we also applied our method of calculation to other geometries considered for the STAR TPC. Figure 13 shows the results for various anode voltages using wires 1m long with a tension of 50g. Qualitatively, they can be summed up by saying that an asymmetric configuration will experience more wire displacement than a symmetric one and the presence of field wires decreases wire displacement at a fixed voltage (while increasing the gas gain and decreasing the pad signal as discussed earlier.)

The wire displacement places constraints on the wire spacing by affecting the spatial uniformity of the gas gain. When the center of an anode wire is displaced with the ends fixed,

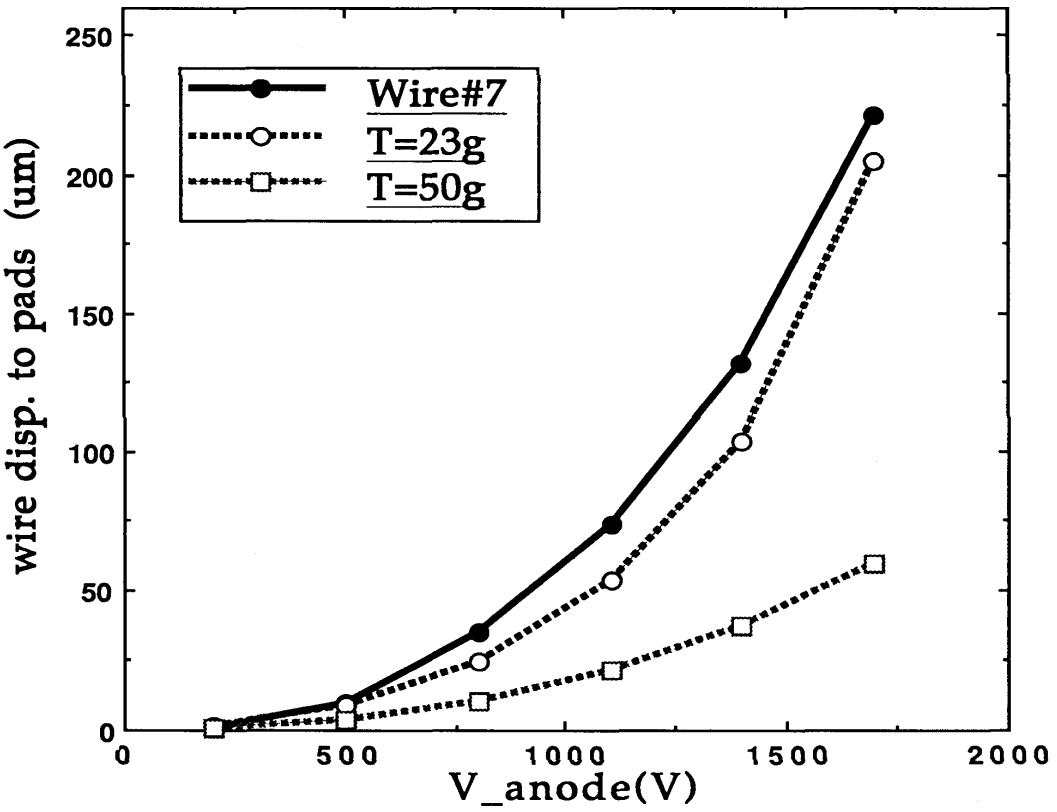

Figure 11. Shown here is the actual displacements of a central wire (#7) on the test structure (at a measured tension of 23g) and the calculated displacements based on GARFIELD.

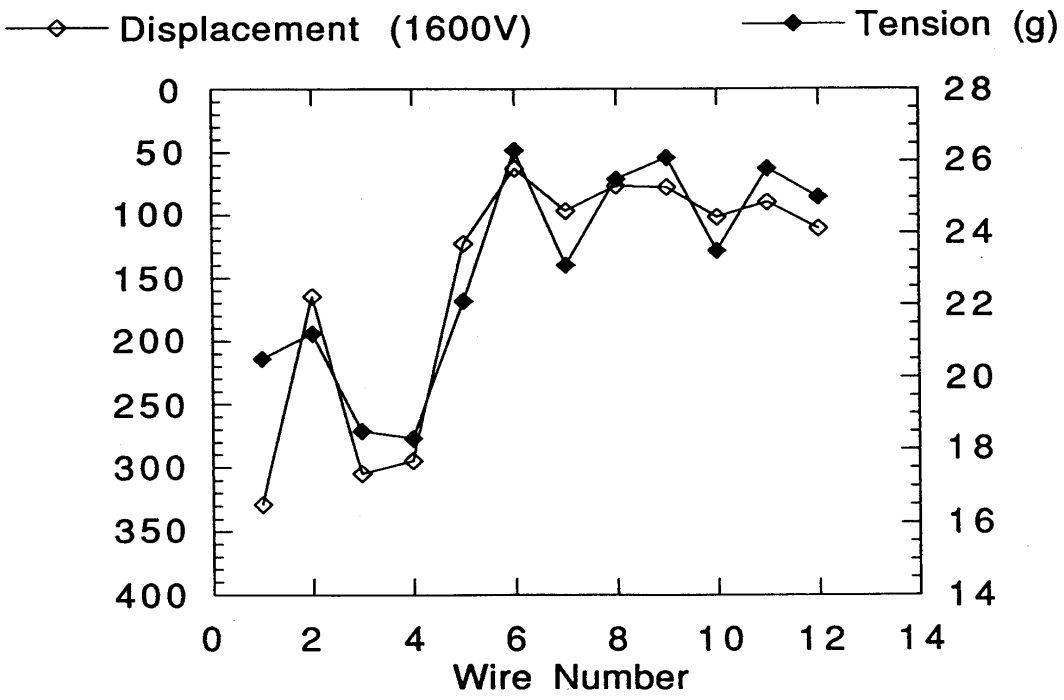

Figure 12. Shown here is the correlation between measured wire displacements and measured wire tensions for our test setup as described in the text.

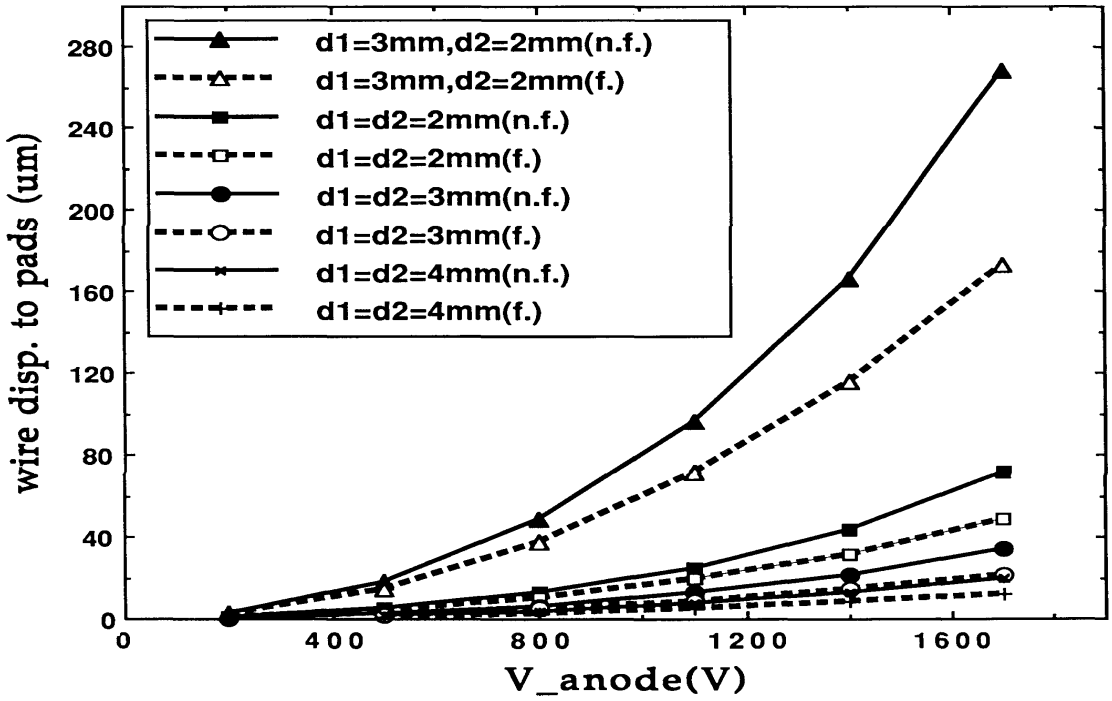

Figure 13. Calculated wire displacements for various chambers as a function of anode voltage. In the legend, f. indicates the presence of field wires, while n.f. indicates their absence. These calculations are done for wires 1m long at a tension of 50g.

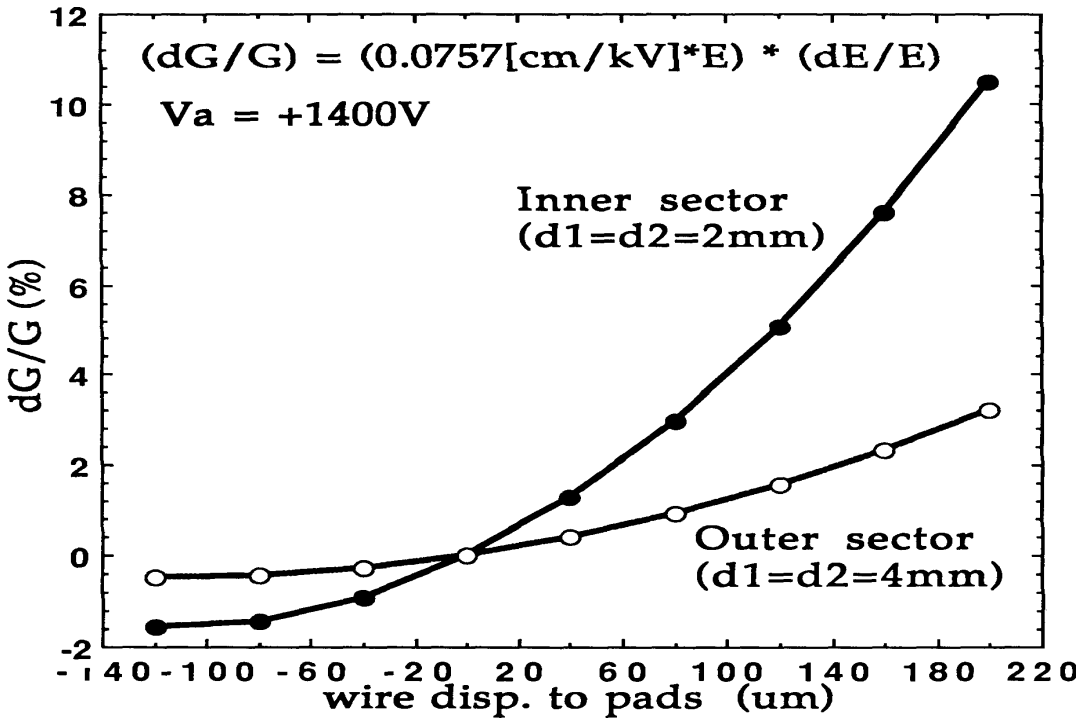

Figure 14. Variation of gain as a function of wire displacement for the STAR TPC configurations.

the surface field strength will vary as a function of position on the wire. According to Equation 2, there should be a corresponding change in the gain. Using GARFIELD again, we calculated the surface field strength at 1400V with several values for the displacement. In figure 14 we show the results for both inner and outer sectors (2mm and 4mm spacings respectively, without field wires). For instance, at 1400V we expect a wire displacement of 40μm (20μm) for the inner (outer) sector from figure 13. The resulting gain variation is about 1% or less for both inner and outer sectors as shown in figure 14. Furthermore, we anticipate operating the inner sectors close to 1200V, so the gain variation should be somewhat smaller.

To further test for displacement effects, an outer sector was constructed with 2-2 wire spacing. Using an outer sector pad plane provides an oversized version of the inner sector. Using an Fe-55 source at various positions over this sector, we see a definite variation in the gain that exceeds any of our calculations or expectations. Figure 15 shows the results normalized to the lowest measured gain for the given conditions. The centers of the wires are at 60cm and the wire lengths and voltages are indicated. There is no clear correlation between voltage and gain variation, but the shorter wires do show a lower variation overall. Another unusual effect was noticed during these tests. The effective gain of the escape peak signals rose faster than for the main peak as the anode voltage was increased. Figure 16 shows these results along with a corresponding set of measurements done on a real outer sector with 4-4 wire spacing. These effects are not well understood at this time.

The second issue of stability is electrical. Operation with double counting, sparking or other forms of discharge is generally unacceptable for STAR. We have conducted tests on these phenomena using the small test chambers and full-size sectors, and we are confident that a 2mm-2mm arrangement is acceptable for the STAR TPC inner sectors. In addition to the aforementioned chambers, we have constructed several others with 2mm-2mm spacing for these tests. These additional 2-2 chambers are similar to the others, but have no pad readout. (They have grounded pads, but no provision for reading them out.) Some of these tests are difficult to

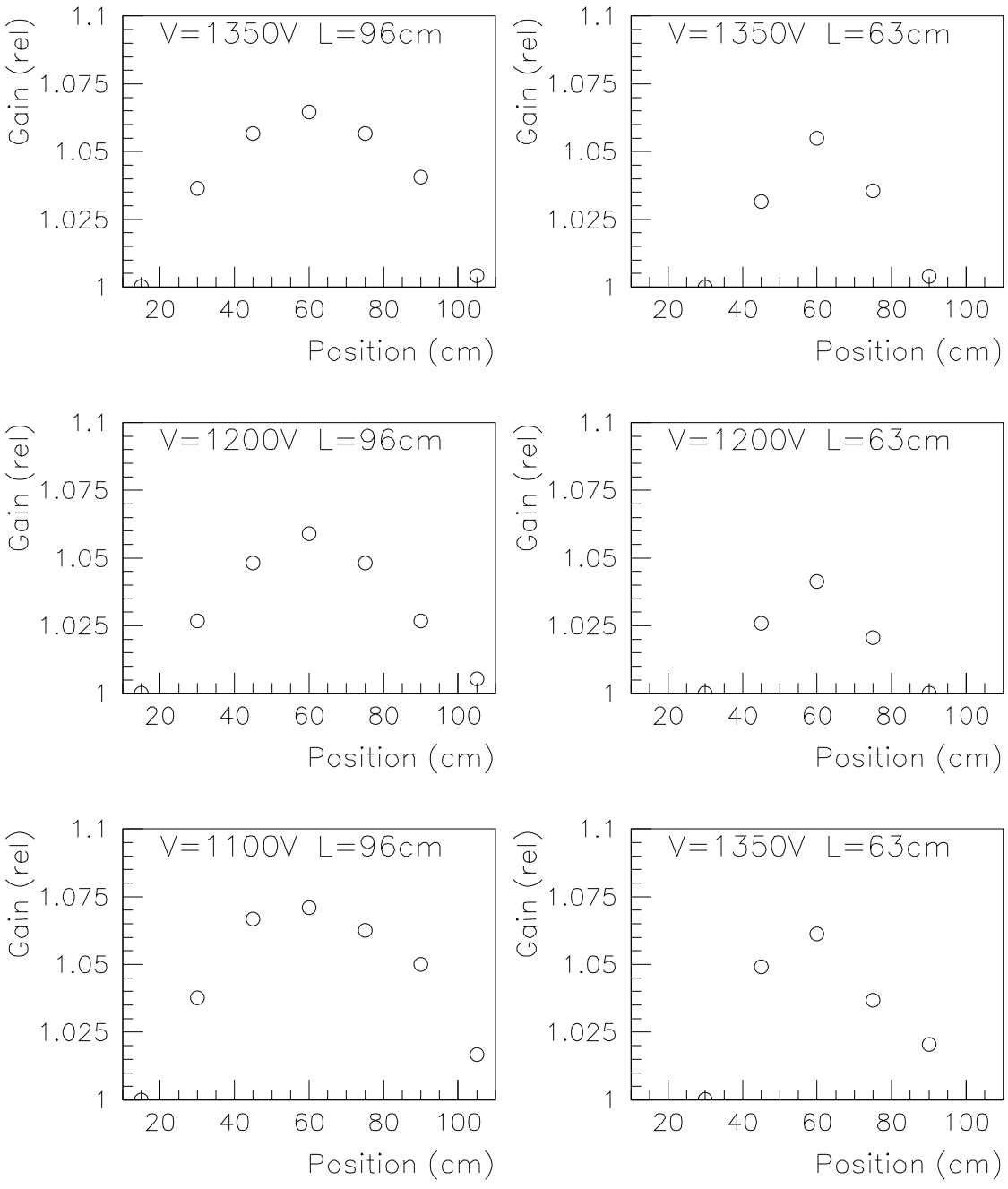

Figure 15. Relative gains as a function of position for two wire lengths and three anode voltages on an outer sector with inner sector spacing (2-2).

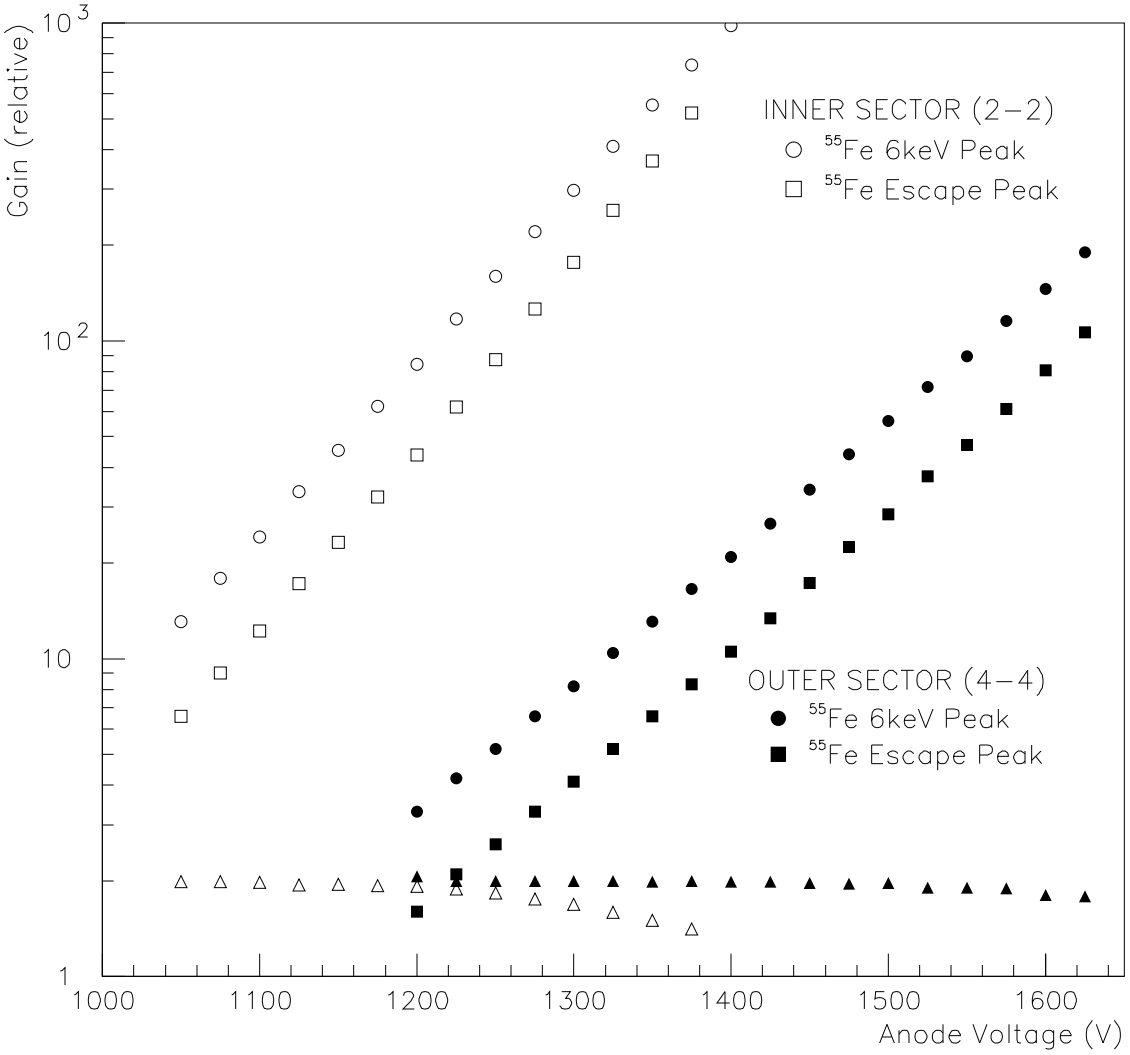

Figure 16. Shown here are the relative gains of the inner and outer sectors, with a comparison between the measured main peak of an ^{55}Fe source and the escape peak. The ratio of main peak height to escape peak height is represented by triangles. The apparent extra increase in gain for the escape peak in the inner sectors at high voltages is not well understood.

quantify and/or had uncontrolled variables that make comparisons less clear, but we will attempt to explain our observations in a useful way.

As has been known for some time, cleanliness is an important issue. Chambers bathed well before use are more resistant to discharge and generally last longer. This is borne out by our tests on these 2-2 chambers. Those bathed before testing would operate normally at 50-100V higher than unwashed chambers built in a typical lab environment with the normal complement of dust and dust-like particles floating around. This lowering of the maximum voltage translates to a lowering of the maximum gain by a factor of 2-4. Sparking and 'glow discharge' (a form of self-sustaining, semi-stable, relatively low current discharge that is sometimes observable as a faint glow on a wire[8,9])) is much more likely to occur in the presence of these contaminants. It could often be induced by exposing the dirty chambers to an 80μCurie Sr-90 β-source. Often when glow discharge was observed, we would be able to see the offending dust particle in the

chamber under a microscope. Hence the decision to build the actual sectors in a clean-room environment is clearly justified. We also attempted to intentionally contaminate the chambers with some of the more likely contaminants from the sector production process. In one instance, we soldered copiously near a chamber (using the same solder as used in the STAR sector production process), sending solder flux all over the place. Many of these little flux balls were visible on the pad plane and several were on the wires. Their presence had a similar effect to that of room dust, that is, a lowering of the maximum operating voltage by about 75V, above which discharge would set in. A similar trial with epoxy (Epon826-Versamid140, as used in the sector construction) showed little effect from the presence of epoxy, at least in the short term on the order of a couple of hours. Longer term effects from charge buildup and wire degradation may be possible though.

For the 2-2 spacing, operation was normal to over 1400V, which gives an effective gain of about 70,000 or an actual gas gain of close to 100,000. Even when exposed to the Sr-90 β source, inducing several microamps of current through the anode wires, the 2-2 chambers could be run at over 1350V without showing any problems after the source was removed. Considering that STAR plans to operate at a gain less than 2000, (an anode voltage of roughly 1125V) there is a large safety margin. Briefly testing other chambers to their limits did not show any clear correlation between wire geometry and maximum operating voltage before discharge. They all were reliable up to gains of at least 50,000.

Finally, we attempted to look for spurious anode signals that might be induced by ionization at the cathode surfaces. To do these tests, we set up a counter to count the signals from the anode wire. Using an Fe-55 source of known activity, we can determine the expected count rate and compare that to the actual count rate. With the iron source, count rate accuracy of about 3% was achievable. Additionally, we used the nitrogen laser with an external trigger and counted the number of triggers. This permitted a higher accuracy in determining the expected count rate. Using counting times on the order of an hour and a trigger rate of about 10Hz, expected count rate accuracies of less than 1% were achieved. The remaining uncertainty comes about from fluctuations in the background counting rate. At expected STAR operating gains (~1000-2000), no deviation from expected count rates was observed for any of the chambers. At gains above 50,000, deviations in the count rate of up to 10% were observed. Attempting to go beyond that by increasing the anode voltage usually resulted in discharge setting in (as described above), and the chamber would no longer operate in a proportional mode. Again, precise quantification of this effect was difficult. There was some variation from day to day and chamber to chamber, but there was no obvious relationship between wire geometry and undesirable effects. With these effects occurring at such high gains, we see no cause for concern from STAR's point of view in using the proposed 2-2 chamber without field wires. Any unwanted effects only occur at levels well beyond the STAR TPC operating levels.

Conclusions

As a result of these various measurements and calculations, we come to several conclusions. Foremost, a 2-2 chamber with the small pads and without field wires satisfies STAR's needs for position resolution, gain uniformity, and signal size in the inner sectors. The outer sector design (4-4) is similarly acceptable. There is a large margin of safety in both mechanical and electrical stability. Additionally, GARFIELD and other computations can be used for easily determining accurate operating characteristics of chambers of this sort.

Chamber d2-d1 (mm)	Pad Size L x W (mm^2)	Gain Fit V_0(V), b(1/V)	PRF Width (mm)	Pad/Anode (%)
1.5-1.5	11.5x2.85	422.5, 0.01255	1.7 ± 0.15	34 ± 2
2-2	11.5x2.85	520.1, 0.01267	1.85 ± 0.1	30 ± 2
2-2fw	11.5x2.85	451.6, 0.01250	1.9 ± 0.1	22 ± 2
2-3	11.5x2.85	487.6, 0.01127	2.0 ± 0.1	38 ± 2
4-4	11.5x2.85	628.7, 0.009341	3.3 ± 0.1	17 ± 2
4-4o	19.5x6.20	628.7, 0.009341	3.7 ± 0.1	34 ± 2

Table 1. Results of several measurements on the small pad test chambers. The various measurements are described in the text.

References

1. Conceptual Design Report for the Solenoidal Tracker at RHIC (STAR), LBL / PUB-5347, June 15, 1992.

2. H. Huang *et al.*, STAR Note 119, Aug. 1993.

3. See for instance, W. G. Gong, STAR Note 103, March 1993.

4. Garfield -- a drift-chamber simulation program by Rob Veenhof, CERN Program Library entry W5050, 1995.

5. T. Alber, *et.al.*, "A Study of Argon, Neon and Helium Based Gas Mixtures for Improving the Spatial Resolution in Time Projection Chambers", Nucl. Instru. Methods A349:1 (1994) 56.

6. W. Blum and L. Rolandi, Particle Detection with Drift Chambers, Springer-Verlag, 1994. (A 'must have' for drift chamber designers and users.)

7. W. G. Gong, STAR Note 104, March 1993.

8. F. Sauli, "Principles of Operation of Multiwire Proportional and Drift Chambers", CERN 77-09, May 3, 1977

9. For an explanation of glow discharge and how it can be put to use in manufacturing processes, see S Wolf and R. N. Tauber, Silicon Processing for the VLSI Era, Vol. 1, Lattice Press, 1986

Some other good references with related material:

D. L. Fancher and A. C. Schaffer, IEEE Trans. Nucl. Sci. NS-26 (1979) 150.
E. Gatti *et al.*, Nucl. Instru. Methods 163 (1979) 83.
E Mathieson, Nucl. Instru. Methods A270 (1988) 602.
A Sobel *et al.*, STAR Note 88, Dec. 1992.